MATERIALS PERFORMANCE IN USC STEAM

Gordon R. Holcomb,[a] Joseph H. Tylczak,[a] and Rongxiang Hu[a,b]
[a]NETL, 1450 Queen Ave SW, Albany, Oregon 97321
[b]URS Corp, P.O. Box 618, South Park, PA 15129

ABSTRACT

Goals of the U.S. Department of Energy's Advanced Power Systems Initiatives include power generation from coal at 60% efficiency, which requires steam conditions of up to 760 °C and 340 atm. Towards this end, further validation of a previously developed chromia evaporation model is shown by examining the reactive evaporation effects resulting from exposure of Haynes 230 and Haynes 282 to moist air environments as a function of flow rate and water content. These two alloys differ in Ti and Mn contents, which may form outer layers of TiO_2 or Cr-Mn spinels. This would in theory decrease the evaporation of Cr_2O_3 from the scale by decreasing the activity of chromia at the scale surface, and be somewhat self-correcting as chromia evaporation concentrates the Ti and Mn phases. The apparent approximate chromia activity was found for each condition and alloy that showed chromia evaporation kinetics. As expected, it was found that increasing the gas flow rate led to increased chromia evaporation and decreased chromia activity. However, increasing the water content in moist air increased the evaporation, but results were mixed with its effect on chromia activity.

INTRODUCTION

Goals of the U.S. Department of Energy's Advanced Power Systems Initiatives include power generation from coal at 60% efficiency, which requires steam conditions of up to 760 °C and 340 atm, so-called advanced ultra-supercritical (A-USC) steam conditions. A limitation to achieving the goal is a lack of cost-effective metallic materials that can perform at these temperatures and pressures. Some of the more important performance limitations are high-temperature creep strength, fire-side corrosion resistance, and steam-side oxidation resistance. Nickel-base superalloys are expected to be the materials best suited for steam boiler and turbine applications above about 675 °C.[1] Specific alloys of interest include Haynes 230 and 282, Inconel 617, 625, and 740, Nimonic 263. Alloy compositions that are the focus of the research presented here are given in Table 1.

Table 1. Nominal alloy compositions (wt%, except for B which is in ppm) and bulk alloy Cr concentrations (C_{Cr}°, mol/m^3) for alloys of interest.[8-10] Source values that were ranges are listed as the midpoint of the range. Source values that were maximums are listed as half the maximum. Only Nb is listed for sources that gave a value or range for Nb+Ta. Source values for Pb, P, S and Bi are omitted.

Alloy	Fe	Cr	Ni	Co	Mo	Ti	Al	Mn	Si	C	Other	C_{Cr}°
Haynes 230	1.5	22	Bal	2.5	2		0.3	0.5	0.4	0.1	0.02 La 14 W 75 B	38000
Haynes 282	0.75	19.5	Bal	10	8.5	2.1	1.5		0.075	0.06	0.15 Cu 50 B	31000
Inconel 740	0.7	25	Bal	20	0.5	1.8	0.9	0.3	0.5	0.03	2 Nb	38700

Steam-side oxidation can result in several adverse effects: general section loss from material thinning, deep localized section loss from internal oxidation (that may also provide crack initiation sites), reduced heat transfer due to the development of insulating oxide layers (that may lead to higher metal temperatures to maintain the same steam conditions), dimensional changes that are critical in airfoils, and downstream erosion from oxide spallation. Evaporation of protective chromia scales may also be an issue at the higher temperatures and pressures of A-USC steam turbines. The evaporation of chromia scales in steam is the focus of the research presented here.

Rapid, or "breakaway" oxidation, can occur from the depletion of Cr in the scale resulting from reactive evaporation of Cr_2O3 in the presence of O_2 and H_2O.[2-5] Clear links to evaporation were shown by how increased gas flow rates led to faster breakaway oxidation and increased Fe:Cr ratios within the oxide scale.[6-7]

In prior work, a methodology to calculate the expected chromia evaporation rate as a function of temperature, pressure, gas velocity, and steam chemistry was developed for chromia forming alloys.[3] The methodology was experimentally validated at low pressures and gas velocities by how well its kinetics predictions matched atmospheric pressure oxidation experiments in air plus water vapor environments. At 760 °C and 340 atm, evaporation rates as high as 5.18×10^{-8} kg/m^2/s of $CrO_2(OH)_2$(g) were predicted for rotating high pressure (HP) turbine blade components.[3] This is equivalent to 0.08 mm per year of solid Cr loss. It was speculated that chromia evaporation upstream of the HP turbine, such as in the superheater, could partially saturate the steam with $CrO_2(OH)_2$(g) and reduce the chromia evaporation rate.

The above efforts were expanded[4] to include 1) the use of new determinations of the thermodynamic properties of $CrO_2(OH)_2$(g),[11] 2) expanding the methodology from flat plate components to cylindrical geometries (such as found within superheaters and steam pipes), 3) linking the chromia evaporation in steam to Cr diffusion within the alloy to predict alloy Cr concentration profiles and breakaway oxidation times, and 4) applying the breakaway oxidation predictions to a hypothetical superheater-steam pipe-HP turbine steam path, where the effects of $CrO_2(OH)_2$(g) saturation along the steam path are applied. In many aspects this was similar to the work of Young and Pint.[5]

Presented here is further validation of the model by examining the reactive evaporation effects resulting from exposure of Haynes 230 and Haynes 282 to moist air environments as a function of flow rate and water content. These two alloys differ in Ti and Mn contents, which may form outer layers of TiO_2 or Cr-Mn spinels, which would in theory decrease the evaporation of Cr_2O_3 from the scale.[12]

CHROMIA EVAPORATION

The oxidation of alloys protected by the formation of Cr_2O_3 (chromia formers) can undergo scale loss due to reactive evaporation of chromium-containing gas species. Water vapor increases the evaporation loss by allowing the formation of $CrO_2(OH)_2$(g), which for these conditions has a higher vapor pressure than CrO_3(g). CrO_3(g) is the predominate Cr gas specie in dry air or oxygen.[13] The formation of $CrO_2(OH)_2$(g) can be written as:

$$\tfrac{1}{2}Cr_2O_3(s) + H_2O(g) + \tfrac{3}{4}O_2(g) = CrO_2(OH)_2(g) \quad (1)$$

The equilibrium partial pressure of $CrO_2(OH)_2$(g) can be found from Eq. 2, where ΔG_1° is the Gibbs energy of reaction 1, R is the gas constant, T is the absolute temperature, K_1 is the equilibrium constant of reaction 1, a_{Cr2O3} is the activity of Cr_2O_3, and P_i is the partial pressure of gas specie i.

$$\Delta G_1^\circ = -RT\ln K_1 = -RT\ln\frac{P_{Cr2(OH)2}}{a_{Cr2O3}^{1/2}P_{H2O}P_{O2}^{3/4}} \quad (2)$$

Even while maintaining a Cr_2O_3 scale, evaporation can change the overall oxidation kinetics from parabolic to linear, or even to breakaway oxidation. Linear kinetics can arise after scale growth from oxidation, which decreases with increasing scale thickness, matches the scale loss from reactive evaporation.[14] The change in scale thickness, x, with time, t, can then be described in terms of the parabolic rate constant, k_p, and the linear reactive evaporation rate, k_e, as:

$$\frac{dx}{dt} = \frac{k_p}{x} - k_e \quad (3)$$

At long times or high reactive evaporation rates, a limiting scale thickness, x_L, arises that is given by:

$$x_L = \frac{k_p}{k_e} \tag{4}$$

In this case metal loss rates are linear, but still involve diffusion through a protective scale. Rapid metal loss can occur when reactive evaporation of Cr depletes the scale (and sometimes the substrate metal) of Cr.[6-7] Decreased Cr in the scale or metal can lead to the formation of less protective oxides, such as Fe-Cr oxides in Fe-Cr base alloys. Unprotective scales can lead to rapid metal loss, or "breakaway" oxidation.

A detailed methodology for calculating evaporation rates in a variety of environments was presented in earlier work for gas flow over a flat plate.[3] Two basic equations were developed: Eq. 5 for laminar flow and Eq. 6 for turbulent flow:

$$k_e\left(\frac{kg}{m^2 s}\right) = 0.664\, Re_L^{0.5} Sc^{0.343} \frac{D_{AB} M_{CrO_2(OH)_2}}{LRT} P_{CrO_2(OH)_2} \tag{5}$$

$$k_e\left(\frac{kg}{m^2 s}\right) = 0.0592\, Re_L^{0.8} Sc^{0.333} \frac{D_{AB} M_{CrO_2(OH)_2}}{LRT} P_{CrO_2(OH)_2} \tag{6}$$

where Re_L and Sc are the dimensionless Reynolds and Schmidt numbers, D_{AB} is the gaseous diffusion coefficient between $CrO_2(OH)_2$ and the solvent gas (m^2/s), $M_{CrO2(OH)2}$ is the molecular mass of $CrO_2(OH)_2$ (kg/g-mol), L is the length (m) in the flow direction of the flat plate, $P_{CrO2(OH)2}$ is the partial pressure of $CrO_2(OH)_2$ (atm), R is the gas constant (8.20594×10^{-5} m^3atm/K g-mol), and T is the absolute temperature (K). The dimensionless Reynolds and Schmidt numbers are defined as:

$$Re_L = \frac{\rho_s u L}{\eta} \tag{7}$$

$$Sc = \frac{\eta}{\rho_s D_{AB}} \tag{8}$$

where ρ_s is the density of the solvent gas (kg/m^3), η is the absolute viscosity (kg/m/s), and u is the gas velocity (m/s). Values for two key parameters in Eqs. 5-8 (D_{AB} and η) are not known and required estimates to be made.[3]

The above methodology for flat surfaces (Eqs. 5-6) was expanded for use in pipes and to include possible saturation effects.[4] Equations 5-6 were written in more general terms that included the average Sherwood number (Sh_{Ave}) and that allowed for the value of the partial pressure of $CrO_2(OH)_2$(g) well away from the metal surface, $P^{\circ}_{CrO2(OH)2}$, to slow down the evaporation (Eqs. 4-5 assumed $P^{\circ}_{CrO2(OH)2}$ was zero), Eq. 9. Here Sh_{Ave} is equal to $0.664Re_L^{0.5}Sc^{0.343}$ for laminar flow over flat plates and to $0.0592Re_L^{0.8}Sc^{0.333}$ for turbulent flow over flat plates.

$$k_e\left(\frac{kg}{m^2 s}\right) = Sh_{Ave} \frac{D_{AB} M_{CrO_2(OH)_2}}{LRT} \left(P_{CrO_2(OH)_2} - P^{\circ}_{CrO_2(OH)_2}\right) \tag{9}$$

For flow within circular tubes, Eq. 9 was used but with a different expression for Sh_{Ave}. For the analysis that follows, the Dittus-Boelter equation[15-16] was used for Sh_{Ave} for turbulent conditions:

$$Sh_{Ave} = 0.023\, Re_d^{0.8} Sc^{0.4} \tag{10}$$

where Re_d is the same as Re_L but with the diameter, d, instead of the plate length, L, in Eq. 7.

One additional point is that the evaporation rate, k_e, from Eq. 9 is for the amount of $Cr_2(OH)_2$(g) leaving the surface, while the mass change data will be in terms of Cr_2O_3(s) lost from the surface. The conversion is shown in Eq. 11.[3] Unless otherwise stated, k_e is on a $Cr_2(OH)_2$(g) basis.

$$k_e[Cr_2O_3] = \frac{M_{Cr2O3}}{2M_{CrO2(OH)2}} k_e[CrO_2(OH)_2] = 0.644 k_e[CrO_2(OH)_2] \quad (11)$$

CHROMIA EVAPORATION IN CYCLIC OXIDATION TESTS

Cyclic oxidation tests were conducted for up to 2000 hourly cycles in moist air. Each hourly cycle consisted of 55 minutes in the furnace, withdrawal from the furnace, holding for 3.4 minutes, and then placement back into the furnace. The remaining 1.6 minutes per hourly cycle was the travel time the samples took into and out of the furnace. The samples experienced rapid heating and cooling rates, and were oriented such that the gas flow was parallel to their surfaces. More experimental details can be found in prior work.[17]

A goal of the cyclic tests was to evaluate alloys for use in A-USC boilers and turbines. Scale exfoliation, resulting in part from thermal expansion mismatch between the alloy and the scale, is an important failure mechanism in boiler tubes.[18] The use of thermal cycles is an aggressive test of scale exfoliation tendencies. While some alloys did exhibit scale exfoliation in the cyclic tests,[17] except as noted no scale exfoliation was observed during tests on the alloys discussed below.

Results for two alloys from prior work,[3-4] Haynes 230 and Inconel 740 at 760 °C, are shown in Table 2. The Haynes 230 results show the influence of gas velocity—a factor of 4 increase in gas velocity resulted in a factor of 2 increase in evaporation, which is consistent with Eqs. 7 and 9. These results were examined with the model, and two apparent chromia activities were found, 0.05 and 0.0006, to describe the behavior. The 0.0006 activity (very low evaporation loss) occurred after a period of higher evaporation loss. A low activity, such as 0.0006, is what is expected from a Cr-containing spinel such as $MnCr_2O_4$.[12]

Table 2. Alloys, conditions, and results for cyclic oxidation tests. Gas flow rates are at temperature. Data for 760 °C are from prior work.[3-4]

Alloy	T, °C	P_{H2O}	Flow Rate, m/s	k_e [Cr_2O_3], kg/m^{2}s	Time Range, hr	Apparent a_{Cr2O3}
Haynes 230	760	0.37	1.9×10^{-3}	3.8×10^{-10}	200-2000	~0.05
Haynes 230	760	0.37	7.6×10^{-3}	11.7×10^{-10}	94-2000	~0.05
Inconel 740	760	0.38	1.9×10^{-3}	1.5×10^{-10}	102-2000	~0.0006
				5.5×10^{-10}	18-734	~0.05
Haynes 230	800	0.19	4.2×10^{-3}	3.4×10^{-10}	200-2000	0.06
Haynes 230	800	0.57	1.0×10^{-3}	4.9×10^{-10}	24-2000	0.14
Haynes 230	800	0.57	4.2×10^{-3}	9.1×10^{-10}	24-2000	0.11
Haynes 282	800	0.19	4.2×10^{-3}	4.9×10^{-10}	600-2000	0.12
Haynes 282	800	0.57	1.0×10^{-3}	6.1×10^{-10}	500-2000	0.21
Haynes 282	800	0.57	4.2×10^{-3}	7.2×10^{-10}	125-1000	0.07

Results for Haynes 230 and Haynes 282 at 800 °C from the current round of test are shown in Figs. 1-2 for two water vapor levels and two gas flow rates, and are also shown in Table 2. The results for Haynes 230 continue to show the same gas velocity dependence shown at 760 °C—a four-fold increase in flow rate doubles the evaporation rate. For Haynes 282, the combination of the highest flow rate and water vapor percentage changed behavior after 1000-12000 cycles. Past this point, small amounts of debris were found upon handling the sample for weighing. So

the mass loss was a combination of chromia evaporation and scale spallation—a chromia evaporation rate was not determined for this time period. A four-fold increase in flow rate increased, but did not double evaporation rate for Haynes 282. It could well be the case that steady state evaporation was not yet reached for the Haynes 282 prior to it starting to spall.

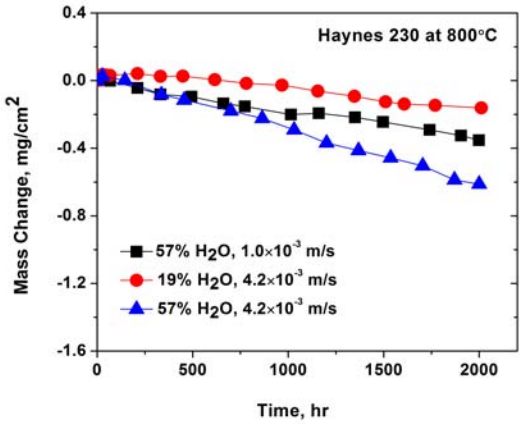

Figure 1. Mass change measurements Haynes 230 at 800 °C in moist air at three different water vapor levels and gas flow rates.

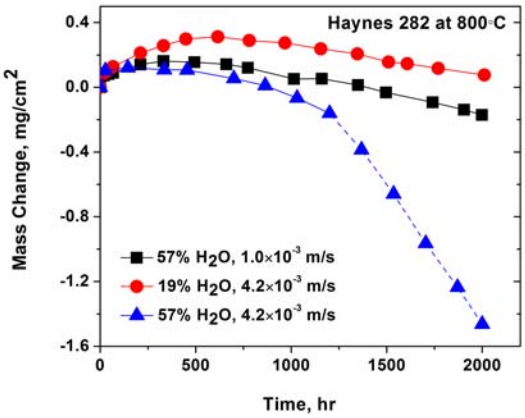

Figure 2. Mass change measurements Haynes 282 at 800 °C in moist air at three different water vapor levels and gas flow rates. The dashed line indicates spalling (no chromia evaporation rates were determined during spalling).

When the results in Figs. 1-2 were compared with the chromia evaporation model, chromia activities were found that matched the results—found in the last column in Table 2. One thought from prior research[4] was that chromia activities would decrease with higher rates of evaporation. As chromia leaves the surface, Mn and Ti oxides would become enriched and thus decrease the chromia activity. Table 2 shows that this is not always the case. Increasing the flow rate, while maintaining a constant P_{H2O}, resulted in chromia activities of Haynes 230 and Haynes 282 dropping from 0.14 to 0.11 and 0.21 to 0.07, respectively. However, raising the P_{H2O} from 0.19 to 0.57 while maintaining a constant flow rate increased the evaporation rate but also increased the chromia activity for Haynes 230 (0.06 to 0.11). The expected result was found for Haynes 282 with an activity decrease from 0.12 to 0.07.

Scanning electron microscopy (SEM) was used to examine the surfaces of the 800 °C samples, Fig. 3. The surface structure of Haynes 230 was finer than that found on Haynes 282. The Haynes 282 at the fastest chromia evaporation rate (lower right-hand image in Fig. 3) shows holes in the structure. One could speculate that these holes were where chromia may have evolved from and thus undercut the outer oxide. This undercutting appears to have resulted in the scale spalling in this sample.

The use of x-ray diffraction (XRD) on these surfaces showed chromia and spinels on Haynes 203 and chromia, spinels, and TiO_2 on Haynes 282. Various Cr-Ni-Mn containing spinels have very similar XRD peaks, making identification of Mn-containing spinels impossible.

Elemental spot analyses on the Haynes 230 surface for the slowest chromia evaporation sample (19% H_2O, 4.2×10^{-3} m/s) did not show any Mn on the surface. Analyses of the other two samples, with higher evaporation rates, showed Mn throughout the surface (along with Cr and O).

Elemental spot analyses on all of the Haynes 282 surfaces showed two distinct types of areas within a fine structure. Figure 4 shows a higher magnification image of this surface and these two types of areas. The smaller grains are primarily Cr and O (with smaller amounts of Ni and Al), and the larger grains (with flat surfaces) to be essentially pure Ti and O.

Additional tests are planned using much higher relative gas velocities. The tests will be conducted in the Hostile Atmosphere Erosion Wear (HAET) apparatus, Figure 5, as described by Tylczak et al.[19] In the HAET, samples are

mounted to the edge of a rotating disk. The disk spins within a controlled atmosphere retort. The velocity at the edge can be as high as 40 m/s. When done in moist air at 760 °C, the expected evaporation rates (based on Eq. 6) are to be of the same order as may be found in the HP A-USC steam turbine (760 °C, 340 atm, and ~300 m/s gas velocity). The resulting microstructures and apparent chromia activities will be determined for conditions closer to that found in an A-USC HP turbine.

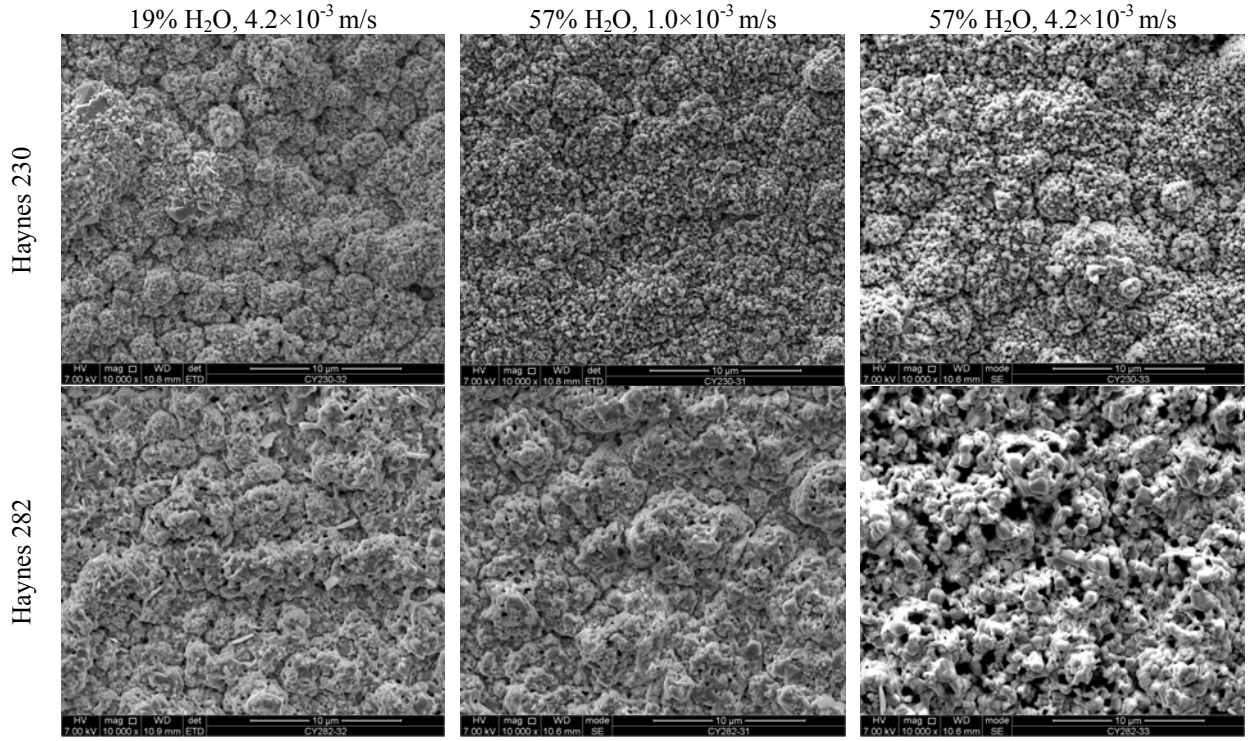

Figure 3. Surface SEM after 2000 cycles at 800 °C in moist air.

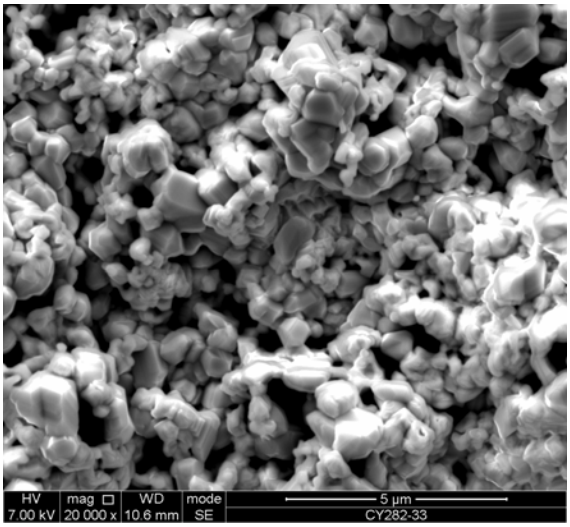

Figure 4. Secondary electron image of the Haynes 282 after 2000 hourly cycles at 800 °C in moist air (57% H_2O) and a gas flow rate of 4.2×10^{-3} m/s. Elemental spot analysis shows the smaller grains to be primarily Cr and O (with smaller amounts of Ni and Al), and the larger grains (with flat surfaces) to be essentially pure Ti and O.

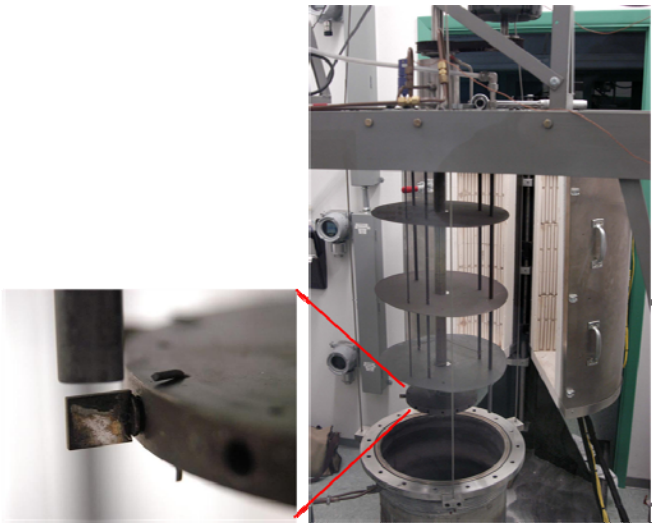

Figure 5. Hostile atmosphere erosion wear (HAET) test apparatus with a sample mounted on the edge of a rotating disk in a controlled atmosphere retort. No erodent will be used for the planned evaporation experiments.

MITIGATION

For the alloys of interest, which contain Ti and/or Mn, large evaporation rates may be self-correcting as chromia is lost from the surface and concentrates Ti and Mn oxides (and thus reduces the chromia activity). Decreases in chromia activity along the steam path can result in little or no evaporation if the steam becomes saturated in $Cr_2(OH)_2$ relative to the lower surface $P_{Cr2(OH)2}$ that arises from the lower a_{Cr2O3}.

Another mitigation would be the use of a non-chromia forming coating. An example would be a thermal barrier coating (TBC), such as one based on yttria stabilized zirconia (YSZ). Such coatings are being postulated for use to reduce turbine blade erosion. This would eliminate the transport path for chromia evaporation. Even if the coating were porous, it would effectively increase the gaseous diffusion boundary layer to the thickness of the coating, thus eliminating much of the detrimental gas velocity effects.

CONCLUSIONS

A methodology was developed to calculate Cr evaporation rates from Cr_2O_3 with a flat planar geometry[3] was expanded upon to allow for interior cylindrical geometries, and to allow for the effects of $CrO_2(OH)_2$ saturation within the gas phase.[4] This approach was combined with Cr diffusion calculations within the alloy (with a constant flux of Cr leaving the alloy from evaporation) to predict Cr concentration profiles as a function of exposure time and to predict the time until the alloy surface concentration of Cr reaches zero.

An important aspect of chromia evaporation in alloys of interest (that contain Mn and Ti) is the possibility of reduced chromia activity at the metal surface. A reduction in chromia activity will reduce chromia evaporation. It was found that increasing the gas flow rate led to increased chromia evaporation and decreased apparent chromia activity. Increasing the water content in the moist air increased the evaporation, but results were mixed with its effect on chromia activity.

REFERENCES

1. Viswanathan, R., Henry, J.F., Tanzosh, J., Stanko, G., Shingledecker, J., Vitalis, B & Purgert, R. (2005). U.S. Program on Materials Technology for Ultra-Supercritical Coal power Plants. *Journal of Materials Engineering and Performance*, Vol. 14, No. 3, (June 2005), pp. 281-292, ISSN 1059-9495.
2. Essuman, E., Meier, G.H., Żurek, J., Hänsel, M. & Quadakkers, W. J. (2008). The Effect of Water Vapor on Selective Oxidation of Fe-Cr Alloys. *Oxidation of Metals*, Vol. 69, Nos. 3-4, (April, 2008), pp. 143-162, ISSN 0030-770X.
3. Holcomb, G.R. (2008). Calculation of Reactive-Evaporation Rates of Chromia. *Oxidation of Metals*, Vol. 69, Nos. 3-4, (April 2008), pp. 163-180, ISSN 0030-770X.
4. Holcomb, G.R. (2009). Steam Oxidation and Chromia Evaporation in Ultrasupercritical Steam Boilers and Turbines. *Journal of the Electrochemical Society*, Vol. 156, No. 9, (September, 2009), pp. C292-C297. ISSN 0013-4651.
5. Young, D.J. & Pint, B.A. (2006). Chromium Volatilization Rates from Cr_2O_3 Scales into Flowing Gases Containing Water Vapor. *Oxidation of Metals*, Vol. 66, Nos. 3-4, (October, 2006), pp. 137-153, ISSN 0030-770X.
6. Asteman, H., Svensson, J.-E., Johansson, L.-G. & Norell, M. (1999). Indication of Chromium Oxide Hydroxide Evaporation during Oxidation of 304L at 873 K in the Presence of Water Vapor. *Oxidation of Metals*, Vol. 52, Nos. 1-2, (August 1999), pp. 95-111, ISSN 0030-770X.
7. Asteman, H., Svensson, J.-E., Norell, M., & Johansson, L.-G. (2000). Influence of Water Vapor and Flow Rate on the High Temperature Oxidation of 304L; Effect of Chromium Oxide Hydroxide Evaporation. *Oxidation of Metals*, Vol. 54, Nos. 1-2, (August 2000), pp. 11-26, ISSN 0030-770X.
8. Haynes International. (2008). Haynes 230 Alloy, H-3135C, Haynes International, Kokomo, IN.
9. Haynes International. (2008). Haynes 282 Alloy, H-3172A, Haynes International, Kokomo, IN.

10. Special Metals Corporation. (2004). Inconel Alloy 740, SMC-090, Special Metals Corporation, Huntington, WV.
11. Opila, E.J., Myers, D.L., Jacobson, N.S., Nielsen, I.M.B., Johnson, D.F., Olminsky, J.K. & Allendorf, M. D. (2007). Theoretical and Experimental Investigation of the Thermochemistry of CrO2(OH)(2)(g). *Journal of Physical Chemistry A*, Vol. 111, No. 10, (October 2007), pp. 1971-1980, ISSN 1089-5639.
12. Holcomb, G.R. & Alman, D.E. (2006). Effect of Manganese Additions on the Reactive Evaporation of Chromium in Ni-Cr Alloys, *Scripta Materialia*, Vol. 54, No. 10, (May, 2006), pp. 1821-1825, ISSN 1059-9495.
13. Graham, H.C. & Davis, H.H. (1971). Oxidation/Vaporization Kinetics of Cr_2O_3. *Journal of the American Ceramic Society*, Vol. 54, No. 2, (February 1971), pp. 89-93. ISSN 0002-7820.
14. Tedman, C.S., Jr. (1966). The Effect of Oxide Volatilization on the Oxidation Kinetics of Cr and Fe-Cr Alloys. *Journal of the Electrochemical Society*, Vol. 113, No. 8, (August 1966), pp. 766-768, ISSN 0013-4651.
15. Winterton, R.H.S. (1998). Where did the Dittus and Boelter Equation Come From? *International Journal of Heat and Mass Transfer*, Vol. 41, Nos. 4-5, (February-March, 1998), pp. 809-810, ISSN 0017-9310.
16. Incropera, F.P. & DeWitt, D.P. (2001). *Fundamentals of Heat and Mass Transfer* (5th edition)., John Wiley & Sons, ISBN 978-0471386506, New York.
17. Holcomb, G.R., Alman, D.E., Doğan, Ő.N., Rawers, J.C., Schrems, K.K. & Ziomek-Moroz, M. (2007). Steam Turbine Materials and Corrosion. *Proceedings of the 21st Annual Conference on Fossil Energy Materials*, Knoxville, TN, April 30-May 1, 2007.
18. Wright, A.I.G. & Tortorelli, P.F. (2007). Program on Technology Innovation: Oxide Growth and Exfoliation on Alloys Exposed to Steam, Report 1013666, EPRI, Palo Alto, CA.
19. Tylczak, J.H., Rawers, J.C., & Adler, T.A. (2004). High Temperature Erosion Testing in a Gasifier Environment. *Proceedings of the 21st Annual Pittsburgh Coal Conference*, paper 49-2, Osaka Japan. September 13-17, 2004, ISBN 1-890977-21-7.